PHYSICAL REVIEW A **90**, 033413 (2014)

Efficient optical schemes to create ultracold KRb molecules in their rovibronic ground state

D. Borsalino,[1] B. Londoño-Florèz,[2] R. Vexiau,[1,3] O. Dulieu,[1] N. Bouloufa-Maafa,[1,4,*] and E. Luc-Koenig[1]

[1]*Laboratoire Aimé Cotton, CNRS, Université Paris-Sud, ENS Cachan, Bâtiment 505, 91405 Orsay-Cedex, France*

[2]*Departamento de Fisíca, Universitad del Valle, Calle 13 N 100-00, Cali, Colombia*

[3]*Institut de Physique de Rennes, Université Rennes 1, Rennes, France*

[4]*UFR de Physique, Université de Cergy-Pontoise, France*

(Received 4 August 2014; published 15 September 2014)

In ongoing experiments ultracold molecules are first created in a weakly bound level of their electronic ground-state manifold, requiring further manipulation with optical fields to transfer them in their absolute ground state. We performed a detailed theoretical analysis of the spectroscopic properties of potassium rubidium diatomic to determine efficient routes for this purpose via stimulated Raman adiabatic passage. We used state-of-the-art molecular potentials, spin-orbit coupling and transition dipole moment to perform our calculations. The dependence of spin-orbit couplings with internuclear distance are of crucial importance as the relevant transitions mainly occur in the chemical bond domain. Two main mechanisms involving a different pair of excited electronic states are modeled and compared for the various isotopologues $^{39}K^{85}Rb$, $^{39}K^{87}Rb$, $^{40}K^{87}Rb$, and $^{41}K^{87}Rb$, starting from the uppermost levels of their lowest triplet state $a^3\Sigma^+$ towards the lowest vibrational level of their ground state $X^1\Sigma^+$. The present model confirms the experimental findings. In addition, it predicts a transfer scheme which involves more efficient transitions.

DOI: 10.1103/PhysRevA.90.033413 PACS number(s): 37.10.Vz, 33.20.−t, 37.10.Mn, 34.20.−b

I. INTRODUCTION

The ability to create in the laboratory samples of dilute atomic gases at ultracold temperatures ($T = E/k_B \ll 1$ mK), where atoms are almost at standstill, represents one of the most fascinating recent developments of atomic physics. Such systems offer long observation time so that measurements with unprecedented precision are achievable. The combined effects of ultralow temperatures (down to the nK scale) and of relatively high number density (up to 10^{14} atoms/cm^3) lead to the spectacular observation of quantum degeneracy in ultracold atomic gases of bosons [1–3] and fermions [4].

In such gases, the existence of long-range anisotropic interactions between the atoms induced by the existence of an intrinsic magnetic dipole moment (nowadays referred to as dipolar gases) is expected to reveal novel physical phenomena [5,6]. The first manifestation of these effects has been demonstrated in experiments dealing with ultracold magnetic atoms like chromium [7,8], erbium [9], or dysprosium [10]. Similar anisotropic interactions are also expected between particles exhibiting an intrinsic permanent electric dipole moment (PEDM), which is a feature of many molecules. This explains the continuously growing interest for achieving a dense sample of ultracold polar molecules [11–13] like diatomic molecules composed of two different alkali-metal atoms which possess a PEDM ranging typically between 0.5 D (for LiNa, KRb) and up to 5.5 D (for LiCs) [14] at the equilibrium distance of their electronic ground state $X^1\Sigma^+$. Such polar molecules are also proposed as attractive candidates for precision measurements like the tests of fundamental theories through the search for the PEDM of the electron [15–19], for parity violation [20], for measurements of fundamental constants [21,22] and of their time variation [23], for quantum information devices [24,25], and for the emergence of a novel ultracold chemistry dominated by quantum effects [26].

Despite the first observation of ultracold Cs_2 molecules in 1998 [27], the formation of ultracold polar molecules in a single quantum state as the initial step for further experimental investigations is still challenging. Due to their complicated internal structure, they cannot be directly laser-cooled just like atoms as they do not exhibit an appropriate closed radiative cycle (except in a few exceptional cases [28–31]). Photoassociation (PA) [32–34], namely, the absorption by an ultracold atom pair of a photon with an appropriate energy, followed by radiative stabilization (RS), has proven very efficient to create sizable samples of ultracold heteronuclear alkali-metal diatomics like KRb [35–37], RbCs [38–40], LiCs [41,42], NaCs [43], and LiRb [44]. In general, the main drawback of such an approach is that the RS step yields molecules in a broad distribution of rovibrational levels in the ground electronic state. To overcome this issue, it was suggested to use a second laser to stimulate the emission down to a specific ground-state level either via a dump pulse (in RbCs, [39]) or to achieve a coherent stimulated rapid adiabatic passage (STIRAP [45,46]) step (in KRb, [47]).

Alternatively, the tunability of Fano-Feshbach resonances (FFRs) with magnetic field [48–50] is routinely used to convert pairs of ultracold atoms into a so-called Feshbach molecule in a well-defined weakly bound energy level related to a dissociation limit defined by a given combination of hyperfine levels of the separated atoms. Interspecies FFRs have been observed in many alkali-metal diatomics (LiNa [51], KRb [52], RbCs [53], LiCs [54,55], LiK [56], NaK [57], NaRb [58], LiRb [59,60]). Such a magnetoassociation (MA) process has proven tremendously efficient to deliver dense samples of ultracold polar molecules in a single quantum level (with KRb [61], LiK [62], RbCs [63,64], NaK [57], NaLi [65]). Thus, it provides the ideal initial step for a coherent transfer via STIRAP of the population down to a single energy level—preferably the lowest one—of the molecular ground state. So far, such a transfer has been

*nadia.bouloufa@u-psud.fr

achieved for the Cs_2[66], Rb_2 [67], KRb [61,68], RbCs [69] species, while a similar goal is currently pursued for most of the other molecular species above. The efficiency of the transfer requires the identification of a two-step Raman transition such that, besides usual angular momenta selection rules for electric dipole allowed transitions, the radial wave function of the intermediate excited level has a favorable overlap with those of the initial state (the Feshbach molecule) and the final one (the lowest level of the ground state).

The purpose of the present paper is to investigate the efficiency of the STIRAP schemes represented in Fig. 1 for several experimentally relevant isotopologues of KRb initially formed in one of the uppermost levels of the lowest metastable triplet state $a^3\Sigma^+$. These schemes involve as the intermediate step a pair of excited molecular states coupled by spin-orbit interaction combining the singlet and triplet characters: (a) the $B^1\Pi$ and $c^3\Sigma^+$ states, and (b) the $b^3\Pi$ and $A^1\Sigma^+$ states (hereafter referred to as the [B-c] and the [b-A] STIRAP schemes, respectively). The experiments of Refs. [61,68] rely on the STIRAP scheme of Fig. 1(e). It is shown that as envisioned in the experiments, the [B-c] STIRAP scheme is generally more efficient than the [b-A] scheme, while this statement may not necessarily be true for all heteronuclear alkali-metal diatomics. The obtained results should guide further experimental investigations to locate various ranges of favorable wavelengths to perform a complete conversion into ground-state molecules of molecules formed by FFR or PA.

The paper is organized as follows. We first recall the main features of the STIRAP calculations in Sec. II based on the mapped Fourier grid Hamiltonian (MFGH) approach [70] for the computation of vibrational energy levels and wave functions. Then in Sec. III we collect all published molecular spectroscopic data for the relevant KRb potential energy curves (PECs) [71–76], combined with up-to-date *ab initio* data for PECs and/or transition electric dipole moments (TEDMs) [77–83] and spin-orbit couplings (SOCs) [77]. Thus,

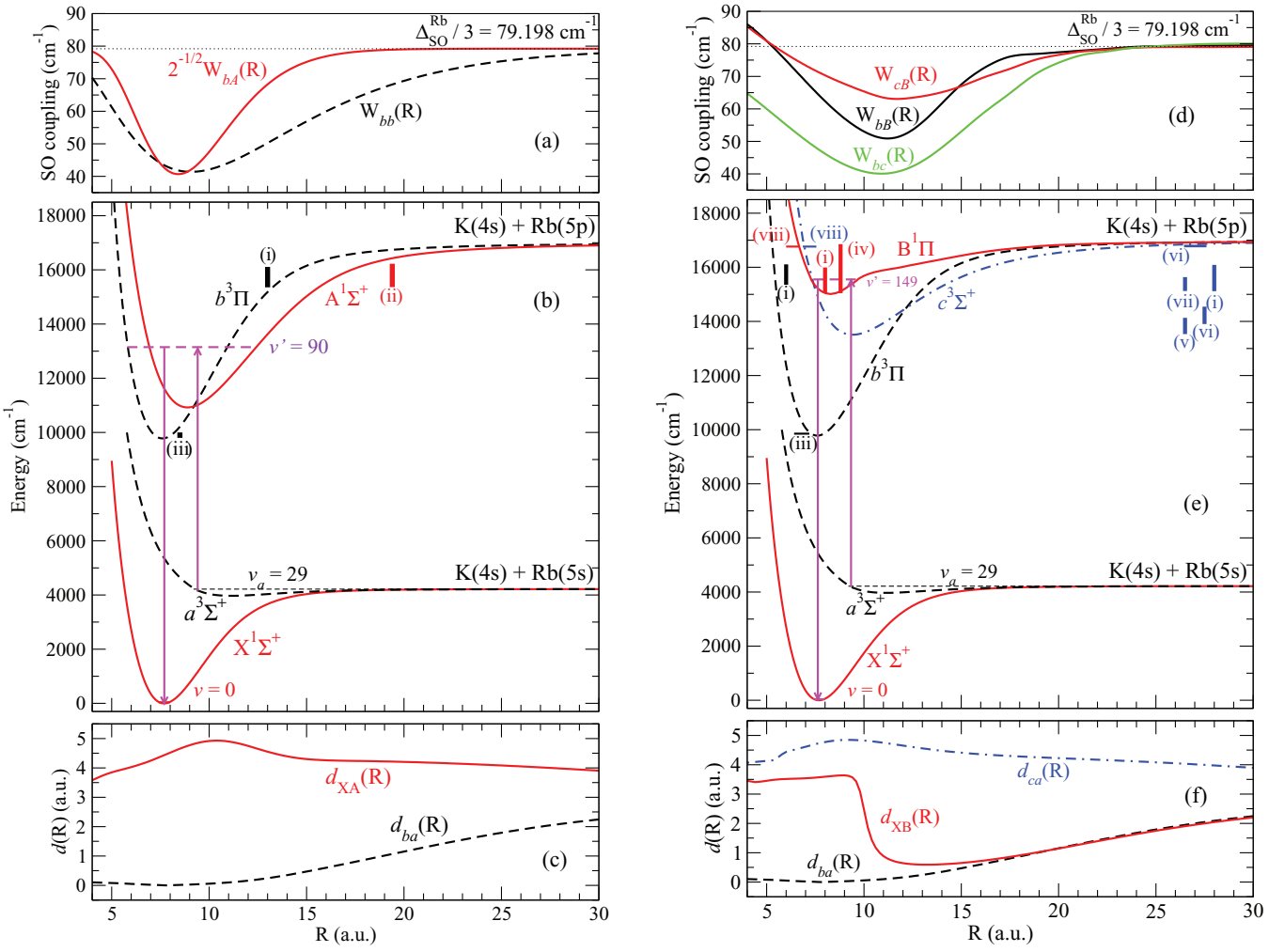

FIG. 1. (Color online) Optimal STIRAP schemes for $^{39}K^{87}Rb$ and relevant molecular data. (Left panels) The [b-A] scheme; (right panels) the [B-c] scheme. (a),(d) R-dependent diagonal and off-diagonal spin-orbit matrix elements coupling the $b^3\Pi$ and $A^1\Sigma^+$ states of panel (b) and the $B^1\Pi$, $c^3\Sigma^+$, and $b^3\Pi$ states of panel (e). (c),(f) Relevant TEDMs for the considered STIRAP schemes. The bibliography for these data is indicated in the text. The optimal intermediate levels for each scheme are reported and connected with upward and downward arrows to the initial $v_a = 29$ level of the $a^3\Sigma^+$ state and to the $v = 0$ level of the $X^1\Sigma^+$ state. The current range of spectroscopic knowledge is indicated with indexed vertical colored bars drawn close to the related PEC: (i) [97]; (ii) [86]; (iii) [31]; (iv) [73]; (v) [75]; (vi) [87]; (vii) [88]; (viii) [37] (see Table I).

we provide an up-to-date description of the KRb molecule which represents a useful database for further investigations. Section IV focuses on the [b-A] STIRAP scheme. There are currently no published experimental results on this scheme, so we restrict our study to the two bosonic isotopologues ^{39}K^{85}Rb and ^{39}K^{87}Rb. We found that around 9100 cm^{-1} for the pump pulse and 13 300 cm^{-1} for the dump pulse—assuming the same laser intensities—Rabi frequencies are of the same order of magnitude ensuring the efficiency of STIRAP to transfer the population from a Feshbach state down to the $v = 0$ ground-state level. Nevertheless, those are quite weak and should require large laser intensities. Section V models the [B-c] STIRAP scheme which has been implemented experimentally for the ^{40}K^{87}Rb and ^{41}K^{87}Rb isotopologues. Our study reveals that a broad range of frequencies, namely, between 9800 and 11 700 cm^{-1} for the pump step and between 14 000 and 15 900 cm^{-1} for the dump step, thus confirming the experimental findings of Refs. [31,61]. The Rabi frequencies are found to be about 10^4 to 10^5 larger than for the [b-A] scheme. Moreover, the combination of the spectroscopic information collected in Refs. [61,84,85] allowed us to predict a new set of optimal vibrational levels for the [B-c] STIRAP scheme. We discuss the huge difference between the [b-A] and the [B-c] schemes on the basis of the peculiar feature of the KRb electronic structure, which may not be reproducible for the other heteronuclear alkali-metal diatomic species.

When appropriate, the atomic unit of length ($1\,a_0 = 0.052\,917\,721\,092$ nm) and of electric dipole moment (1 a.u. = 2.541 580 59 D) is used.

II. MODEL FOR STIRAP WITH KRb MOLECULES

A. STIRAP basics

The STIRAP technique has been extensively discussed [45,46]. In a three-level system in Λ configuration, it allows a coherent transfer of the population between an initial level $|i\rangle$ and a final level $|g\rangle$ which cannot be directly coupled by a laser field. The trick consists of coupling these levels to an intermediate level $|e\rangle$ with a pump and a dump laser pulse of frequency $\omega_{i,e}$ [$\omega_{e,g}$] and a time-dependent Rabi frequency $\overline{\Omega}_{i,e}(t)$ [$\overline{\Omega}_{e,g}(t)$]. When the two-photon Raman resonance condition is fulfilled, one of the instantaneous eigenstates of the system, the *dark* level, is a coherent superposition of $|i\rangle$ and $|g\rangle$ only, so that the population can be transferred without loss due to spontaneous emission of the—usually short-lived—$|e\rangle$ level. To achieve the full population transfer, the two laser pulses must have a well-defined phase relation with no fluctuations, implemented through a counterintuitive time sequence where the dump pulse overlaps the pump pulse but starts before it. Moreover the maximum value of the two Rabi frequencies should be equal to allow for the adiabatic following of the dark state. In a diatomic molecule like KRb, the Rabi frequency for a transition between two levels $|j\rangle$ and $|j'\rangle$ is expressed as

$$\overline{\Omega}_{jj'} = \langle j|\vec{d}(R)\cdot\vec{E}_0|j'\rangle/\hbar,$$

where $\vec{d}(R)$ is the R-dependent TEDM and $\vec{E}_0$ the time-dependent electric field with maximum amplitude $\overline{E_0}$. Determining the most efficient STIRAP transfer scheme for a given pair of levels $|i\rangle$ and $|g\rangle$ consists of finding the $|e\rangle$ level for which the Rabi frequencies $\overline{\Omega}_{i,e}(t)$ and $\overline{\Omega}_{e,g}(t)$ are sufficiently large and of the same order of magnitude. Let us emphasize, that it is possible to vary independently the intensities of the pump and dump laser pulses to reach the strict equality between the two Rabi frequencies.

Let us emphasize that we applied several approximations in our model, most of them depending on the chosen experimental conditions, and which are not crucial for our purpose. First, the polarizations of the pump and dump lasers are not considered. Consequently, the rotation $\vec{\ell}$ of the molecular axis in the laboratory frame is disregarded, as well as the relevant Höln-London factors in the related matrix elements. Furthermore, the STIRAP processes depicted in Fig. 1 rely on a pump transition taking place mainly around the inner turning point of the $a^3\Sigma^+$ state where the perturbation of the nodal structure of radial wave functions induced by the hyperfine or Zeeman couplings with the $X^1\Sigma^+$ state is negligible.

B. The choice of the initial levels in KRb

In the following the final level will always be the $v = 0$ vibrational level of the $X^1\Sigma^+$ ground state of KRb, i.e., $|g\rangle \equiv |X, v = 0\rangle$. The initial level depends on the association process chosen to form the molecules from laser-cooled atoms, resulting in different optimal schemes for the STIRAP transfer.

Ni *et al.* [61] successfully achieved the conversion of cold atom pairs from a dense gas of ^{40}K fermions and ^{87}Rb bosons into ^{40}K^{87}Rb $|X, v = 0\rangle$ fermionic molecules through MA followed by a STIRAP step. The vibrational wave function of the Feshbach molecule, with typical binding energy of a few hundred kHz, has been identified as being very close to that of the level $|a^3\Sigma^+; v_a = 30\rangle$ [77,87,89]. This Feshbach molecule is also denoted by $\overline{v}_a = -2$, where the vibrational quantum number $\overline{v}_a$ is counted downward from the dissociation limit. Furthermore, these Feshbach molecules have been converted via a highly efficient (84%) STIRAP step into $\overline{v}_a = -3$ molecules bound by more than 10 GHz [87,90]. Therefore, according to the approximations described above, we will consider as initial levels the uppermost levels of the $a^3\Sigma^+$ state, namely, $|i\rangle = |a, v_a = 29\rangle$, $|a, v_a = 30\rangle$, and $|a, v_a = 31\rangle$. They correspond to $\overline{v}_a = -3, -2$, and -1, respectively, except for ^{41}K^{85}R, which possesses 33 bound levels in the a state due to its large scattering length.

In a different experiment, Aikawa *et al.* created $a^3\Sigma^+$ ^{41}K^{87}Rb bosonic molecules in $v_a \sim 20$–25 levels by PA followed by radiative decay [88]. The population is generally distributed over a large number of rotational and hyperfine levels, but the hyperfine mixing is less significant for such levels bound by $\sim$15 cm^{-1}. We also consider the initial state $|i\rangle = |a, v_a = 21\rangle$ as representative of this case.

In the Supplemental Material attached to the present paper [91], the energy levels and squared transition matrix elements for the STIRAP schemes with $|i\rangle = |a, v_a = 20$–$31\rangle$ are reported for the most commonly studied isotopologues ^{39}K^{85}Rb, ^{39}K^{87}Rb, ^{40}K^{87}Rb, and ^{41}K^{87}Rb. Data concerning other v_a values or isotopologues are available on request.

C. The choice of the intermediate levels in KRb and their modeling

The $|e\rangle$ levels must belong to an electronic state with mixed triplet and singlet characters, connected to the $|i\rangle = |a, v_a = 20\text{–}30\rangle$ and $|g\rangle = |X, v = 0\rangle$ levels through electric dipole transitions with large matrix elements, i.e., large TEDM and good Franck-Condon factors (FCFs). As stated above, we investigate two STIRAP schemes, based on two different sets of intermediate excited electronic states coupled by spin-orbit interaction (Fig. 1). The [b-A] scheme relies on the $b^3\Pi$ and $A^1\Sigma^+$ coupled states leading to a pair of $\Omega = 0^+$ states in Hund's case c notation, correlated to the $\mathrm{K}(4^2S_{1/2}) + \mathrm{Rb}(5^2P_{1/2,3/2})$ dissociation limits. The notation Ω denotes the absolute value of the projection of the total electronic angular momentum on the molecular axis. This case has been considered in the first theoretical searches [92,93] for reliable STIRAP schemes. The [B-c] scheme actually involves three coupled molecular states, namely $B^1\Pi$, $c^3\Sigma^+$, and $b^3\Pi$, inducing states of $\Omega = 1$ symmetry dissociating to the same asymptotes $\mathrm{K}(4^2S_{1/2}) + \mathrm{Rb}(5^2P_{1/2,3/2})$. The successful experiment of Ref. [61] proceeded through this scheme. We restrict our investigations up to moderately excited levels to avoid exploring complex and dense spectra in the upper range of the corresponding PECs.

D. The spin-orbit coupling matrices

The structure of the matrix representation of the spin-orbit operator $\hat{W}_{\mathrm{so}}^{\Omega}$ coupling the $b^3\Pi$ and $A^1\Sigma^+$ states for $\Omega = 0^+$ and the $B^1\Pi$, $c^3\Sigma^+$, and $b^3\Pi$ states for $\Omega = 1$ are displayed, for instance, in Ref. [94], where the constant SOCs related to the Rb fine structure splitting $\Delta_{\mathrm{so}}^{\mathrm{Rb}} = 237.594\ \mathrm{cm}^{-1}$ are here replaced by R-dependent functions displayed in Figs. 1(c) and 1(e) and specified in Sec. III B.

We thus have for $\Omega = 0^+$

$$\hat{W}_{\mathrm{so}}^{0} = \begin{array}{c} \\ |b\rangle \\ |A\rangle \end{array} \begin{array}{c} \begin{array}{cc} |b\rangle & |A\rangle \end{array} \\ \begin{pmatrix} -W_{bb}(R) & W_{bA}(R) \\ W_{bA}(R) & 0 \end{pmatrix} \end{array}, \tag{1}$$

and for $\Omega = 1$

$$\hat{W}_{\mathrm{so}}^{1} = \begin{array}{c} \\ |c\rangle \\ |b\rangle \\ |B\rangle \end{array} \begin{array}{c} \begin{array}{ccc} |c\rangle & |b\rangle & |B\rangle \end{array} \\ \begin{pmatrix} 0 & W_{cb}(R) & W_{cB}(R) \\ W_{cb}(R) & 0 & -W_{bB}(R) \\ W_{cB}(R) & -W_{bB}(R) & 0 \end{pmatrix} \end{array}. \tag{2}$$

E. Calculation of vibrational wave functions

The vibrational levels of the $X^1\Sigma^+$ and $a^3\Sigma^+$ electronic states are described in a single-channel picture ($N = 1$), with the Hamiltonian $\hat{H}_{X,a} = \hat{T} + \hat{V}_{X,a}(R)$, where $\hat{T}$ is the nuclear kinetic-energy operator and $\hat{V}_X(R)$ and $\hat{V}_a(R)$ the Born-Oppenheimer potentials for these states.

The vibrational levels of the coupled $\Omega = 0^+$ and $\Omega = 1$ electronic states are extracted from a two-channel ($N = 2$) and a three-channel ($N = 3$) representation. The Hamiltonian of the system is then $\hat{H}_{\Omega} = \hat{T} + \hat{V}_{\Omega}(R) + \hat{W}_{\mathrm{so}}^{\Omega}(R)$. In this expression the matrix representation of $\hat{V}$ is diagonal and contains the PECs for the b and A states ($\Omega = 0$) and for the B, c, and b states ($\Omega = 1$).

The eigenvalues and eigenvectors of $\hat{H}_{X,a}$ and $\hat{H}_{\Omega}$ are calculated by expressing them with the MFGH method, based on a spatial grid with a step adjusted to the local de Broglie wavelength with a scaling parameter $\beta = 0.4$ (see Refs. [70,95] for more details), extending from $R_{\mathrm{min}} = 5a_0$ to $R_{\mathrm{max}} = 300a_0$, and containing up to $N_G = 566$ grid points. We have checked that the chosen value of R_{max} is sufficiently large to allow the correct description of the uppermost bound level of the $a^3\Sigma^+$ state, in particular for the $^{41}\mathrm{K}^{85}\mathrm{Rb}$ isotopologue with the largest positive scattering length $a_L = 349.8a_0$ [76], i.e., with the last bound level very close to the dissociation limit with a large R extension. Our calculated binding energy for this level agrees within a few percent with the value $-0.000\,275\ \mathrm{cm}^{-1}$ predicted by the quantum defect theory (QDT) law or Ref. [96] for a $1/R^6$ long-range potential.

The representation of the Hamiltonians thus involves squared matrices of $N \times N_G$ order, which, after diagonalization, yield energies $E(v'_{\Omega})$ and radial wave functions for the vibrational levels of the system. Energy levels of the coupled states are labeled with a *global* index v'_{Ω} increasing with decreasing binding energy, and have a mixed b and A character (for $\Omega = 0^+$) and B, c, and b character (for $\Omega = 1$). The eigenfunctions for a given Ω value are expressed as linear combinations of the related coupled electronic states $|j\rangle$ weighted by radial wave functions $\psi_j^{\Omega v'_{\Omega}}(R)$ according to

$$|\Omega;\, v'_{\Omega}\rangle = \sum_{j=1}^{N} \frac{1}{R} \psi_j^{\Omega v'_{\Omega}}(R)\, |j\rangle\,, \tag{3}$$

with the normalization condition

$$\sum_{j=1}^{N} \int_0^{\infty} \left|\psi_j^{\Omega v'_{\Omega}}(R)\right|^2 dR \equiv \sum_{j=1}^{N} \varpi_j^{\Omega v'_{\Omega}} = 1. \tag{4}$$

In the following we sometimes use a different index $v_{\Omega}^{\prime(j)}$ (with $j = b, A, B, c, b$) to refer to a level with a prevailing "j" character assigned through the largest weight $\varpi_j^{\Omega v'_{\Omega}}$ in the expansion of Eqs. (3) and (4) (see, for instance, Table I, and Sec. III C). This assignment may be completed by considering the rotational constant

$$\begin{aligned} B_{\Omega\, v'_{\Omega}} &= \langle \Omega; v'_{\Omega} | \hbar^2/(2\mu R^2) | \Omega; v'_{\Omega} \rangle \\ &= \sum_{j=1}^{N} \int_0^{\infty} \frac{\hbar^2}{2\mu R^2} \left|\psi_j^{\Omega v'_{\Omega}}(R)\right|^2 dR \end{aligned} \tag{5}$$

and the energy spacing between neighboring levels

$$\Delta G\left(v_{\Omega}^{\prime(j)}\right) = E\left(v_{\Omega}^{\prime(j)} + 1\right) - E\left(v_{\Omega}^{\prime(j)}\right). \tag{6}$$

F. Transition matrix elements

The Rabi frequency for the pump (dump) transition is proportional to the TME which involves the vibrational functions $\varphi_a^{v_a}$ (φ_X^{v}) of the $a^3\Sigma^+$ ($X^1\Sigma^+$) state and the triplet (singlet) part of the coupled wave function of the intermediate level $|\Omega; v'_{\Omega}\rangle$ [Eq. (3)]

$$\begin{aligned} d_{j_t a}^{v'_{\Omega} v_a} &= \langle \Omega; v'_{\Omega} | \hat{d}_{j_t a} | a; v_a \rangle \\ &= \int_0^{\infty} \psi_{j_t}^{\Omega v'_{\Omega}}(R)\, d_{j_t a}(R)\, \varphi_a^{v_a}(R) dR \end{aligned} \tag{7a}$$

TABLE I. Available spectroscopic data for the excited electronic states of various KRb isopotologues correlated to the K(4s) + Rb(5p) dissociation limit (also depicted in Fig. 1). The studied energy range is given with respect to the minimum of the ground electronic state $X^1\Sigma^+$ with the related range of assigned vibrational quantum numbers $v_\Omega'^{(j)}$. The root mean square deviation (rms) $\Delta_{\rm rms}$ between experimental and calculated level energies is also reported.

Electronic state	Isotopologue	Energy range (cm^{-1})	$\Delta_{\rm rms}$ (cm^{-1})
$A^1\Sigma^+_{\Omega=0^+}$	^{39}K^{85}Rb	$15\,363.43 \leqslant E_{v'^A_{0^+}} \leqslant 16\,224.36$	3.26
	[86]	$93 \leqslant v'^A_{0^+} \leqslant 122$	
$b^3\Pi_{\Omega=0^+}$	^{39}K^{85}Rb	$15\,526.69 \leqslant E_{v'^b_{0^+}} \leqslant 16\,037.76$	3.00
	[97]	$91 \leqslant v'^b_{0^+} \leqslant 104$	
$c^3\Sigma^+_{\Omega=1}$	^{39}K^{85}Rb	$13\,531.42 \leqslant E_{v'^c_1} \leqslant 14\,132.73$	0.384
	[75]	$0 \leqslant v'^c_1 \leqslant 13$	
	^{40}K^{87}Rb	$13\,903.17 \leqslant E_{v'^c_1} \leqslant 14\,545.01$	3.17
	[87]	$8 \leqslant v'^c_1 \leqslant 23$	
	^{39}K^{85}Rb	$15\,116.18 \leqslant E_{v'^c_1} \leqslant 16\,087.40$	7.33
	[97]	$38 \leqslant v'^c_1 \leqslant 71$[a]	
	^{41}K^{87}Rb	$15\,124.50 \leqslant E_{v'^c_1} \leqslant 15\,636.13$	5.52
	[88]	$39 \leqslant v'^c_1 \leqslant 55$	
$b^3\Pi_{\Omega=1}$	^{39}K^{85}Rb	$15\,355.10 \leqslant E_{v'^b_1} \leqslant 16\,107.34$	2.06
	[97]	$87 \leqslant v'^b_1 \leqslant 106$	
$B^1\Pi_{\Omega=1}$	^{39}K^{85}Rb	$15\,043.19 \leqslant E_{v'^B_1} \leqslant 16\,854.67$	4.6
	[73]	$0 \leqslant v'^B_1 \leqslant 31$[b]	
	^{39}K^{85}Rb	$15\,043.05 \leqslant E_{v'^B_1} \leqslant 15\,993.45$	4.25
	[97]	$0 \leqslant v'^B_1 \leqslant 20$	

[a]Our vibrational assignment v'^c_1 differs by four units from the one of Ref. [97].
[b]Levels with $v_B \leqslant 25$ only are included in the rms (see text).

$$d^{vv'_\Omega}_{X j_s} = \langle X; v_X|\hat{d}_{X j_s}|\Omega; v'_\Omega\rangle = \int_0^\infty \varphi^v_X(R)\, d_{X j_s}(R)\, \psi^{\Omega v'_\Omega}_{j_s}(R) dR, \quad (7b)$$

where the indexes j_t and j_s refer to the triplet and singlet electronic states coupled in a given Ω symmetry, and $d_{j_t a}(R)$ and $d_{X j_s}(R)$ are the R-dependent TEDM for the pump and dump transitions. For $\Omega = 0^+$ we have $j_t = b$ and $j_s = A$, while for $\Omega = 1$ we have $j_t = b$ or c, and $j_s = B$. The squared matrix elements $|d^{v'_\Omega v_a}_{j_t a}|^2$ and $|d^{vv'_\Omega}_{X j_s}|^2$ determine the efficiency of the STIRAP process and are systematically calculated in Secs. IV and V for both STIRAP schemes above.

III. MOLECULAR STRUCTURE AND SPECTROSCOPIC DATA FOR KRb

In the following, we build a representation of the KRb potential curves from a combination of available spectroscopic data (collected in Table I) and results from accurate *ab initio* calculations. We display in Table II a summary of the piecewise construction of these PECs, explained in details in Secs. III A and III C. In addition, TEDMs and SO couplings are taken from several sources based on *ab initio* calculations (Secs. III B and III D). All the molecular data used in our calculations are given in the Supplemental Material attached to the present paper [91].

A. Building the potential energy curves piecewise

The $X^1\Sigma^+$ and $a^3\Sigma^+$ electronic states of the ^{39}K^{85}Rb and ^{39}K^{87}Rb molecules have been extensively studied experimentally by various spectroscopic techniques [71,74]. Numerous perturbations due to the hyperfine structure (HFS) were observed for levels lying close to the K(4s) + Rb(5s) dissociation limit. More recently, several Feshbach resonances have been measured in cold ^{40}K^{87}Rb molecules [99]. We use here the X and PECs which have been derived from a coupled-channel model [76], yielding an accurate analytical form valid for any combination of K and Rb isotopes, and over all internuclear distances from $5a_0$ up to $4000a_0$. In the following, the origin of energies is taken at the minimum of the $X^1\Sigma^+$ potential. The K(4s) + Rb(5s) dissociation limit is then located at 4217.822 cm^{-1} [100].

The excited electronic states converging toward the K(4^2S) + Rb(5^2P_J) dissociation limits (the $J = 1/2$ limit being located at 16 796.8 cm^{-1} [100]) are strongly perturbed by the large spin-orbit interaction resulting in complicated spectra. Thus, experimental spectroscopic data are fragmentary and mainly concern the high energy range 13 000–16 500 cm^{-1}. However, a Rydberg-Klein-Rees (RKR) potential curve for the bottom of the $B^1\Pi$ [72,73] and the $c^3\Sigma^+$ [75] wells have been derived by standard spectroscopic analysis. It is worthwhile to mention that the recent production of ultracold molecules by MA [87] or PA [86,88,97] provided information on more excited vibrational levels with $\Omega = 0^+$ and $\Omega = 1$ symmetries.

TABLE II. Piecewise PECs used in our calculations, built from experimental and *ab initio* data. *Ab initio* may be globally shifted either in energy by Δ_j^0 ($j = A,b,B$) to minimize the rms deviation between calculated and experimental energies of the vibrational levels (see Table I), in energy by Δ_c^1 and in distance by $\Delta_{R,c}^1$ (for $c^3\Sigma^+$) to match the experimental energy minimum and equilibrium distance of the PEC, or by Δ_B^1 (for $B^1\Pi$) to account for the difference between the minima of the calculated $B^1\Pi$ and the fourth $\Omega = 1$ PEC. The asymptotic part is described by a multipolar expansion in (C_n/R^n) ($n = 6, 8$). A cubic spline interpolation is used between two successive nonadjacent R domains.

$X^1\Sigma^+$		Experiment [76]		
$a^3\Sigma^+$		Experiment [76]		
$b^3\Pi$		$R \leqslant 19.8a_0$ *ab initio* [83] $\Delta_b^0 = -17.5$ cm^{-1}		$R \geqslant 25.0a_0$ R^{-n} expansion [98]
$A^1\Sigma^+$		$R \leqslant 25.0a_0$ *ab initio* [83] $\Delta_A^0 = +10.0$ cm^{-1}		$R \geqslant 35.0a_0$ R^{-n} expansion [98]
$c^3\Sigma^+$	$R < 7.85a_0$ *ab initio* [83] $\Delta_c^1 = -22.2$ cm^{-1} $\Delta_{R,c}^1 = +0.053a_0$	$7.85a_0 \leqslant R \leqslant 11.65a_0$ experiment [75]	$11.65a_0 < R \leqslant 30a_0$ *ab initio* [83] $\Delta_c^1 = -22.2$ cm^{-1} $\Delta_{R,c}^1 = +0.053a_0$	$R \geqslant 40a_0$ R^{-n} expansion [98]
$B^1\Pi$	$R < 6.8a_0$ *ab initio* [83] $\Delta_B^1 = -8.2$ cm^{-1}	$6.8a_0 \leqslant R \leqslant 19.1a_0$ experiment [72,73] $\Delta_B^1 = -8.2$ cm^{-1}	$19.1a_0 < R \leqslant 20.0a_0$ *ab initio* [83] $\Delta_B^1 = -8.2$ cm^{-1} $R \leqslant 21.7a_0$	$R \geqslant 30.0a_0$ R^{-n} expansion [98] $R \geqslant 27.9a_0$

The spectral windows experimentally investigated for different KRb isotopologues are summarized in Table I and depicted in Fig. 1. Note that the two lowest levels $v_{0^+}^{\prime(b)} = 0,1$ located around 9800 cm^{-1} have been observed only very recently [31] and have not been incorporated in the present work.

Due to the lack of experimental data, accurate *ab initio* calculations are necessary to complete the construction of the PECs for the excited states. In the present work, we construct piece by piece the PECs at small and intermediate interatomic distance by combining the RKR potentials above with the accurate PECs computed in our group [83]. Our approach employs large effective core potentials and core polarization potentials accounting for the K^+ and Rb^+ ionic cores and is based on full configuration interaction for the two valence electrons built from a large Gaussian basis sets [14,101]. The repulsive energy between the Rb^+ and K^+ cores,

$$V_{cc}(R) = 720.125\exp(-2.107\,93\,R)$$

(in a.u.) [102,103], is added to the calculated PECs. Finally, all the PECs are connected through a spline interpolation to an asymptotic expansion $-C_6/R^6 - C_8/R^8$ where the C_6 and C_8 coefficients are taken from Ref. [98]. Details on the piecewise construction of the PECS are displayed in Table II.

B. Spin-orbit interaction

The matrix elements of the $\hat{W}_{\rm so}^0$ and $\hat{W}_{\rm so}^1$ defined in Sec. II D are represented in Figs. 1(a) and 1(d). At large internuclear distance, they are expressed in terms of the spin-orbit constant of the Rb atom $A/2 = \Delta_{\rm SO}^{\rm Rb}/3 = 79.198$ cm^{-1}.

For $\Omega = 0^+$ [Eq. (1)], there is no available spectroscopic nor theoretical determination of the diagonal $W_{bb}(R)$ and off-diagonal $W_{bA}(R)$ couplings. Thus, we used those of the NaRb molecule [104] also involving Rb and therefore correctly describing at large R distances the splitting between the $K(4^2S) + Rb(5^2P_J)$ asymptotes. We assumed that as Na is the nearest alkali metal of K, the couplings at small R are similar in NaRb and KRb.

For $\Omega = 1$ [Eq. (2)], the off-diagonal elements $W_{cb}(R)$, $W_{cB}(R)$, and $W_{bB}(R)$ are taken from the *ab initio* calculations of Ref. [77].

C. Adjustment of the potential energy curves

The diagonalization of the Hamiltonian of Sec. II E including the above PECs and couplings yields energy levels v_Ω' and their composition in terms of electronic states.

For $\Omega = 0^+$, the resulting levels v_{0^+}' are ascribed to the series of perturbed levels arising either from $A^1\Sigma^+$ (if $\varpi_A^{0^+v_{0^+}'} > 1/2$) or from $b^3\Pi$ ($\varpi_b^{0^+v_{0^+}'} > 1/2$) and are labeled with the index $v_{0^+}^{\prime(A)}$ or $v_{0^+}^{\prime(b)}$, respectively. The energy spacing between neighboring levels of a given series $\Delta G(v_{0^+}^{\prime(A)})$ and $\Delta G(v_{0^+}^{\prime(b)})$ [Eq. (6)] is in good agreement with the experimental results of Ref. [86] in the former case and of Ref. [97] in the latter case for the $^{39}K^{85}Rb$ molecule, justifying the $v_{0^+}^{\prime(A)}$ and $v_{0^+}^{\prime(b)}$ assignments. Before connecting them to their asymptotic limit, we shifted the *ab initio* $A^1\Sigma^+$ or $b^3\Pi$ PECs by Δ_A^0 and Δ_b^0 in order to minimize the residuals between the calculated and experimental energies of the perturbed levels. A cubic spline interpolation is used to connect two adjacent domains at small, intermediate, and asymptotic range. The obtained rms for the residuals amounts to about 3 cm^{-1} for the studied range of levels (see Table I).

The $b^3\Pi$ PEC determined above is then used for the $\Omega = 1$ case. The RKR curve of the $c^3\Sigma^+$ state [75] is matched to our *ab initio* curve at short and intermediate distances after shifting it in energy by $\Delta_c^1 = -22.2$ cm^{-1} and in distance by $\Delta_{R,c}^1 = 0.053a_0$ to match the experimental spectroscopic constants.

The case of the $B^1\Pi$ state is slightly more involved. We use the RKR potential [72,73] given over a wide range of distances and energies and we connect it at small and intermediate R to the *ab initio* potential. An energy shift $\Delta_B^1 = -8.2$ cm^{-1} is applied to *both* the RKR and the *ab initio* curves for $R \leqslant 21.7a_0$ in order to minimize the rms between calculated energies and experimental energies measured in Ref. [97] for ^{39}K^{85}Rb. Shifting the RKR curve of Refs. [72,73] is actually not surprising. Indeed, this RKR curve is extracted from observed $B^1\Pi$ levels extending from the bottom of the potential ($T_e = 15\,012.493$ cm^{-1}) up to levels lying $\sim$100 cm^{-1} above the K(4^2S) + Rb($5^2P_{1/2}$) dissociation limit at 16 796.8 cm^{-1}. The PEC is therefore assigned to the fourth $\Omega = 1$ state [hereafter denoted 4(1)] correlated to the K(4^2S) + Rb($5^2P_{3/2}$) limit at 17 034.4 cm^{-1}. Due to the strong SOC the calculated 4(1) curve is shifted upwards compared to the isolated $B^1\Pi$ PEC. The downward shift Δ_B^1 of the RKR curve thus approximately compensates this effect and our model correctly reproduces the $B^1\Pi$ levels with $v'_B \leqslant 25$ observed in Refs. [73,97], with an rms of about 4 cm^{-1}. In addition, the *ab inito* calculations reveal that there is an anticrossing between the $B^1\Pi$ and $(2)^1\Pi$ PECs around $9.5a_0$ and around 15 550 cm^{-1}. Our model does not take into account this feature. Thus, we consider that our description of the $\Omega = 1$ states is valid only for vibrational levels with energy smaller than the anticrossing energy location.

The assignment of the $|\Omega = 1; v'_1\rangle$ levels resulting from the interaction between the $b^3\Pi$, $c^3\Sigma^+$, and $B^1\Pi$ states, in terms of $v_1^{\prime(B)}$, $v_1^{\prime(c)}$, and $v_1^{\prime(b)}$ labels is sometimes delicate. For instance, the weights $\varpi_j^{1v'_1}$ ($j = B,c,b$) may be almost equal for strongly coupled levels. This assignment is also constrained by the necessity to avoid large irregularities in the level spacing or in the rotational constants. Table I displays the rms between calculated and experimental energies for levels assigned to the three $\Omega = 1$ states in various isotopologues: ^{39}K^{85}Rb [73,86,97], ^{40}K^{87}Rb [87], and ^{41}K^{87}Rb [88].

D. Transition electric dipole moments

The TEDMs $d_{XA}(R)$ and $d_{XB}(R)$ between singlet states and $d_{ba}(R)$ and $d_{ca}(R)$ between triplet states are obtained from our *ab initio* calculations [83] and are displayed in Figs. 1(c) and 1(f). The rapid decrease of $d_{XB}(R)$at $R \sim 5a_0$ is due to the avoided crossing between the $B^1\Pi$ potential and the next $(2)^1\Pi$ potential. This pattern is in agreement with the results of Leininger *et al.* [79], while the variation reported by Kotochigova [77] is smoother and occurs over a broader R domain $7.5a_0 < R < 12.5a_0$. We emphasize that in the considered energy range, smaller than 16 300 cm^{-1}, the relevant parts of the potential wells of the excited PECs do not extend beyond $R = 20a_0$, so that such a difference in the TDMs should lead to different results for the optimal STIRAP transitions. Note also that $d_{ca}(R)$ is larger than $d_{ba}(R)$ by more than a factor 400, so that the [B-c] STIRAP scheme is expected to be more favorable than the [b-A] one.

IV. THE [b-A] STIRAP SCHEME WITH $\Omega = 0^+$ LEVELS

Owing to the lack of experimental data for this scheme, we restrict our study to the most abundant bosonic species ^{39}K^{85}Rb and to the bosonic ^{39}K^{87}Rb species, which is currently widely investigated. Also, we only discuss the STIRAP schemes starting from the $v_a = 29$ level (with a binding energy of 0.270 cm^{-1} = 8.084 GHz) and the $v_a = 31$ level (with a binding energy of 0.005 64 cm^{-1} = 169 MHz). We recall that level energies are generally given with respect to the bottom of the $X^1\Sigma^+$ PEC, unless otherwise stated.

First we can invoke simple arguments based on the Franck-Condon (FC) principle to easily locate favorable intermediate levels allowing the implementation of a STIRAP scheme. The $A^1\Sigma^+$and $b^3\Pi$ PECs cross each other at $R \sim 9.1a_0$. From usual intuition, efficient transitions are expected to occur toward levels v'_{0^+} with an energy close to the crossing location, where strong triplet-singlet mixing takes place, thus enhancing transition probabilities with both the initial v'_a levels and the $v = 0$ level [92,93]. Furthermore, as suggested in Fig. 1(b), an efficient pump transition is expected to occur mainly at the inner turning point of the $a^3\Sigma^+$ PEC at $R_a = 9.273a_0$, populating 0^+ levels with a turning point around R_a. This leads to the selection of the $v'_{0^+} = 19$ level at the energy 11 031.70 cm^{-1} [or a binding energy of 5910 cm^{-1} with respect to the K($4s$) + Rb($5p$) limit]. This level lies about 73 cm^{-1} above the [b-A] crossing and indeed presents an almost equal singlet-triplet mixing. However, a look at Fig. 1(c) reveals that the TEDM $d_{ba}(R)$ almost vanishes for $R \leqslant 15a_0$, i.e., in a range covering the $b^3\Pi$ well. This feature induces transition matrix elements for the pump and dump transitions which differ by a huge 2×10^{-6} factor ($|d_{ba}^{19,31}|^2 \sim 1.7 \times 10^{-8}$ and $|d_{XA}^{0,19}|^2 \sim 8.3 \times 10^{-3}$), thus preventing any implementation of an efficient STIRAP scheme. We come back to this peculiar feature of KRb in the Concluding Remarks.

A. Transition matrix elements in the 0^+ symmetry

The FC principle being invalid for selecting an efficient STIRAP scheme, it is necessary to perform a systematic search for possible STIRAP schemes looking at any intermediate level v'_{0^+}. Using the data of Sec. III we computed their binding energies and the corresponding excitation energies, their mixing weights [Eq. (3)], and their squared TMEs [Eqs. (7a) and (7b)] for the pump and dump transitions. All these results are reported in the Supplemental Material attached to this paper for the ^{39}K^{85}Rb and ^{39}K^{87}Rb isotopologues [91].

The squared TMEs are displayed in Fig. 2 for the ^{39}K^{87}Rb species, on a doubly scaled graph with both the pump and the dump transition energies. We recall that these energies are evaluated by neglecting any HFS, which is a reasonable assumption for the present purpose. The general trends of the variation are similar for all isotopologues not shown here.

The change of the initial level from $v_a = 31$ to $v_a = 29$ simply results in a global increase of the squared TMEs by a factor of about 10. Indeed, the magnitude of the TMEs is mainly determined by the short-range part of the v_a wave functions, only differing by a normalization factor for these levels close to the dissociation limit. It should be noted also that including the hyperfine interaction would bring, in principle, another scaling factor depending on the amount of triplet state in the chosen initial level (for instance, the one of the Feshbach molecule). Thus, we assume here that for the sake

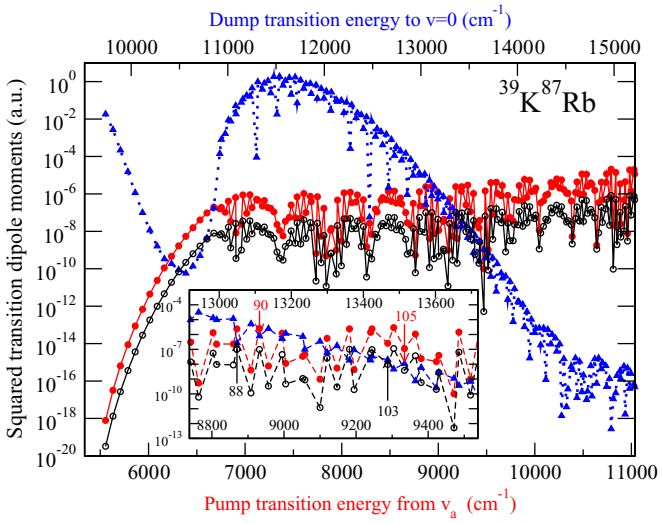

FIG. 2. (Color online) Computed squared matrix elements $|d_{ba}^{v'_{0^+}v_a}|^2$ as a function of pump transition energy (bottom horizontal axis) and $|d_{XA}^{vv'_{0^+}}|^2$ as a function of dump transition energy (top horizontal axis) of the $^{39}K^{87}Rb$ TEDM relevant for the [b-A] STIRAP scheme through $\Omega = 0^+$ intermediate levels v'_{0^+}. The pump transition starts from the $v_a = 29$ (solid red circles) and $v_a = 31$ (open black circles) levels of $a^3\Sigma^+$, towards vibrational levels v'_{0^+} of the $A^1\Sigma^+$ and $b^3\Pi$ coupled states located well below the $K(4^2S_{1/2}) + Rb(5^2P_{1/2})$ limit. The dump transition (blue triangles) starts from those levels to end into the $v = 0$ level of the $X^1\Sigma^+$ ground state. The inset enlarges the most favorable region where both matrix elements are nearly equal. The intermediate levels $v'_{0^+} = 88$ and $v'_{0^+} = 103$ (reached from $v_a = 31$) and $v'_{0^+} = 90$ and $v'_{0^+} = 105$ (reached from $v_a = 29$) correspond to optimal efficiency. The pump transition frequency toward $v'_{0^+} = 103$ and $v'_{0^+} = 105$ are close to the one of a 1064-nm laser.

of experimental efficiency the initial wave function has a pure triplet character.

For pump transition energies below 7000 cm^{-1}, only low-lying levels in the $b^3\Pi$ well can be reached from the uppermost $a^3\Sigma^+$, but their radial wave functions are located at distances smaller than R_a so that the overlap with v_a wave functions is negligible. Above $E_{pump} = 7000$ cm^{-1}, the transition enters the zone of the avoided crossing. The combination of reasonable wave-function overlap, mixed b-A character of the 0^+ levels, and still weak TEDM results in squared TMEs reaching a range of 10^{-6}–10^{-5} a.u., with a slow increase when increasing energies. The oscillatory pattern of the squared TMEs is induced by the interference between the radial wave functions involved in the TME integral [Eq. (7)], as well as the alternate main triplet or singlet weight of the 0^+ levels.

Figure 1(b) shows that the $X^1\Sigma^+$ and $b^3\Pi$ PECs are surprisingly similar, which induces a fairly diagonal FC matrix for such a spin-forbidden transitions. Besides, the $v'_{0^+} = 0$ level, readily assigned to $v'^{(b)}_{0^+} = 0$, contains a few percent of singlet character with a wave function very similar in shape to the one of the triplet component. This results in a surprisingly high squared TME of about 0.01 a.u., enhanced also by the high value of the d_{XA} function [about 4.5 a.u.; see Fig. 1(c)] in the related R range. Note that this peculiar feature, together with the long radiative lifetime (several μs) of the $v'^{(b)}_{0^+} = 0$ level (which cannot decay to any of the $a^3\Sigma^+$ levels which lie in a different R domain, while the TEDM is very low, as already stated), is at the core of the proposal for a narrow-line laser cooling of $^{41}K^{87}Rb$ molecules in the rovibrational ground level [31].

For $v'_{0^+} > 0$ levels, the squared TMEs for the dump transition decrease with the spatial overlap between the final $v = 0$ wave function and the v'_{0^+} ones. They increase again when reaching the region of the [A-b] crossing (around $E_{dump} = 11\,000$ cm^{-1}) as the v'_{0^+} levels acquire a strong singlet component. Their magnitude culminates at about 2 a.u. around $E_{dump} = 11\,500$ cm^{-1}, thus being 10^6 larger than the squared TMEs for the pump transitions.

B. Identification of the optimal 0^+ levels for STIRAP

Figure 2 shows that the squared TMEs of the pump and dump transitions cross each other in two energy regions. A first sharp crossing occurs for $v'_{0^+} = 15$ ($v'^{(b)}_{0^+} = 15$) for $E_{pump} = 6675.1$ cm^{-1} and $E_{dump} = 10\,854.9$ cm^{-1}, with a quite weak squared TME of about 10^{-7} a.u. A somewhat more favorable region is shown in the inset of Fig. 2, where a compromise between the low magnitude of the $d_{ba}(R)$ function and the weak spatial overlap between the $v = 0$ and the singlet component of the v'_{0^+} wave functions is reached. The detailed information on the most favorable STIRAP process for the $^{39}K^{85}Rb$ and $^{39}K^{87}Rb$ species is given in Table III. For convenience, both the excitation energy and the binding energy with respect to $K(4s) + Rb(5p)$ are reported in the table. The latter energy can readily be related to the $K(4^2S_{1/2}) + Rb(5^2P_{1/2})$ limit by subtracting $(2/3)\Delta_{so}^{Rb} = 158.398$ cm^{-1}.

We selected two optimal 0^+ levels in $^{39}K^{87}Rb$, namely, $v'_{0^+} = 90$ and $v'_{0^+} = 105$ for implementing a STIRAP scheme. The latter has a main singlet character and involves a pump transition energy close to the one offered by a conventional laser at 1064 nm, but with weak squared TMEs of about 10^{-8} a.u. The former level, with a main triplet character, has squared TMEs, with the $v_a = 29$ level and the $v = 0$ level about 100 times larger, and should definitely be recommended in this situation. The table confirms that similar conclusions can be drawn for the other level $v_a = 31$ and the other isotopologue $^{39}K^{85}Rb$. Obviously, other combinations of levels could be identified using the Supplemental Material [91], providing that the chosen laser intensities for the pump and dump transitions compensate the difference in the squared TMEs (as has been experimentally demonstrated, for instance, for the $^{87}Rb^{133}Cs$ molecule [105]).

V. THE [B-c] STIRAP SCHEME WITH $\Omega = 1$ LEVELS

The theoretical model is expected to be more accurate in this case due to the large amount of available spectroscopic data concerning the $c^3\Sigma^+$and $B^1\Pi$ coupled states visible in Fig. 1 [31,37,72,73,75,86–88,97], which allowed us to improve the quality of the PECs (Sec. III C). Note that this is the motivation for naming the presently investigated STIRAP scheme by the labels of these two states. In addition, only little spectroscopic information is available for the $b^3\Pi$

TABLE III. Summary of the characteristics of the optimal transitions for the [b-A] STIRAP scheme through $\Omega = 0^+$ intermediate levels v'_{0^+} in ^{39}K^{85}Rb and ^{39}K^{87}Rb. Pump transition from $v_a = 29,31$ $a^3\Sigma^+$ levels are considered. The dump transition ends at $v = 0$ of the $X^1\Sigma^+$ state. Both binding energy $E_{\rm bind}$ [relative to the K($4s$) + Rb($5p$) dissociation limit], and excitation energy $E_{\rm exc}$ (relative to the minimum of the $X^1\Sigma^+$potential well) of the v'_{0^+} levels are given, with the weight of the A and b components [Eq. (3)]. The energies $E_{\rm pump}$ and $E_{\rm dump}$ and the related squared transition dipole moments $|d_{ba}^{v'_{0^+}v_a}|^2$ and $|d_{XA}^{vv'_{0^+}}|^2$ of the pump and dump transitions are also reported. Numbers in parentheses hold for powers of 10.

Initial level	^{39}K^{85}Rb		^{39}K^{87}Rb			
v_a	31	29	31		29	
Intermediate level						
v'_{0^+}	99	90	88	103	90	105
$E_{\rm bind}$ (cm^{-1})	3544.8	3795.2	3868.2	3450.1	3805.7	3403.4
$E_{\rm exc}$ (cm^{-1})	13 410.4	13 160.0	13 087.0	13 505.1	13 149.5	13 551.8
$\varpi_b^{0^+v'_{0^+}}$	0.928	0.903	0.926	0.092	0.921	0.058
$\varpi_A^{0^+v'_{0^+}}$	0.072	0.097	0.074	0.908	0.079	0.942
Pump transition						
$E_{\rm pump}$ (cm^{-1})	9192.5	8942.4	8869.2	9287.3	8932.0	9334.2
$\left\|d_{ba}^{v'_{0^+}v_a}\right\|^2$ (a.u.)	7.7 (−8)	1.2 (−6)	9.9 (−8)	9.74 (−9)	1.35 (−6)	5.54 (−8)
Dump transition						
$E_{\rm dump}$ (cm^{-1})	13 372.5	13 122.2	13 049.3	13 467.4	13 111.8	13 514.0
$\left\|d_{XA}^{vv'_{0^+}}\right\|^2$ (a.u.)	2.3 (−8)	7.5 (−7)	2.75 (−7)	2.0 (−8)	8.0 (−7)	1.1 (−8)

state [31,84]. Figure 1(f) also shows that large TMEs are anticipated for both the pump and the dump transitions as both relevant TEDMs $d_{ca}(R)$ and $d_{XB}(R)$ amount to several atomic units in the region of the inner turning point of the $a^3\Sigma^+$ state and of the bottom of the $B^1\Pi$ and $X^1\Sigma^+$ PECs.

In contrast with the previous case, several attempts to implement the desired STIRAP transfer relying on $\Omega = 1$ levels have been achieved. The first successful experiment concerns the fermionic ^{40}K^{87}Rb species created by MA through a Feshbach resonance in a level that can be assigned to a good approximation to the $v_a = 30$ (or $\overline{v}_a = -2$) $a^3\Sigma^+$ level. In a second step, the molecules were transferred to $v = 0$ with an efficiency larger than 90% [61,87,106]. The chosen intermediate level was the $v_1'^{(c)} = 23$ (coupled) level of the $c^3\Sigma_1^+$ at 14 544.8 cm^{-1}.

A recent proposal [88] starts from the $v_a = 21$ $a^3\Sigma^+$ level bound by -15.90 cm^{-1} below the K($4s$) + Rb($5s$) limit in the bosonic ^{41}K^{87}Rb molecule. This level is initially populated by PA followed by spontaneous emission. The spectroscopic properties (including HFS) of $\Omega = 1$ coupled levels with a strong $c^3\Sigma^+$ character ($39 \leqslant v_1'^{(c)} \leqslant 55$) lying in the 15 124.9–15 636.6 cm^{-1} energy range were carefully analyzed, revealing TMEs large enough for being intermediate levels of a STIRAP scheme.

An optimal STIRAP pathway in ^{39}K^{85}Rb has been identified with a purely spectroscopic investigation, i.e., by combining two independent spectra probing the same excited states reached from both v_a $a^3\Sigma^+$ levels and from the $v = 0$ $X^1\Sigma^+$ level [84]. Let us note that such an approach does not provide the mixture of B, c, and b character of the excited level [85]. Thus, starting from $v_a = 21$, the $v_1'^{(B)} = 7,8$ excited levels are good candidates for an efficient STIRAP transfer.

In the present section, STIRAP schemes starting from $v_a = 21$ and $v_a = 29$ levels and using intermediate $\Omega = 1$ levels are systematically modeled for the species of experimental interest ^{39}K^{85}Rb, ^{39}K^{87}Rb, ^{40}K^{87}Rb, and ^{41}K^{87}Rb.

A. Transition matrix elements in the Ω = 1 symmetry

The TMEs for the pump transitions from $v_a = 29$ and for the dump transition to $v = 0$ are displayed in Fig. 3(a) for the ^{41}K^{87}Rb isotopologue. At the pump step, both $b^3\Pi$ and $c^3\Sigma^+$ components of the intermediate level can be excited and the corresponding TMEs are separately drawn. For pump transition energies below ∼9300 cm^{-1}, corresponding to the bottom of the $c^3\Sigma^+$ PEC, the TMEs $|d_{ba}^{v'_1v_a}|^2$ (black trace) are almost identical to the results for $|d_{ba}^{v'_{0^+}v_a}|^2$ in Fig. 2. The $|d_{ca}^{v'_1v_a}|^2$ curve (red trace) follows a similar variation, as the $c^3\Sigma^+$ component of these levels is small (with a weight smaller than 0.0015), and similar to the one of the $b^3\Pi$ component. However, it is still larger than $|d_{ba}^{v'_1v_a}|^2$ due to the $d_{ca}(R)$ larger than $d_{ba}(R)$ by about two orders of magnitude. Above ∼9300 cm^{-1}, the $|d_{ca}^{v'_1v_a}|^2$ TMEs suddenly increase as the $c^3\Sigma^+$ levels are reached, resulting in a large spatial overlap of the vibrational wave functions. The $|d_{ba}^{v'_1v_a}|^2$ TMEs remain at the same level because the $b^3\Pi$ vibrational wave functions are more and more oscillatory. As for $\Omega = 0^+$, these curves are strongly oscillating according to the alternate main character ($j_t = b$ or c) of the corresponding levels.

The first points of $|d_{BX}^{v'_10}|^2$ are very similar to those reported in Fig. 2. Then the TMEs are negligible, revealing a very small admixture of B character in the v'_1 levels until $E_{\rm dump} \sim 13\,500$ cm^{-1}, corresponding to the lowest $v_1'^{(c)}$ levels. A strong coupling is then induced by the large spin-orbit interaction taking place at the crossing between the $B^1\Pi$ and $c^3\Sigma^+$ curves around $7.3a_0$. In addition, the TEDM is large, $d_{XB}(R) \sim 3.5a_0$,

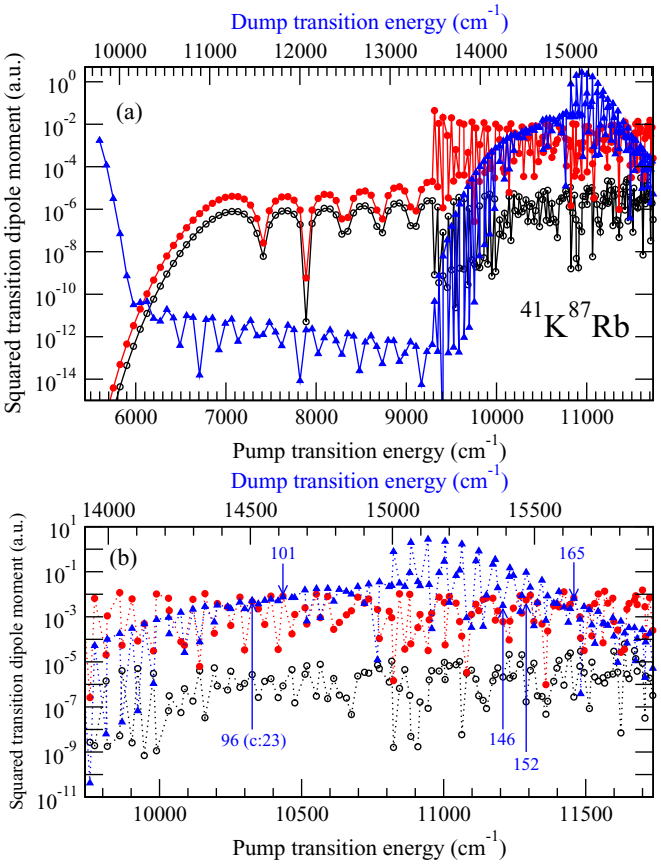

FIG. 3. (Color online) (a) Computed squared matrix elements $|d_{j_t a}^{v_1' v_a}|^2$ as a function of pump transition energy (bottom horizontal axis) and $|d_{XB}^{v v_1'}|^2$ as a function of dump transition energy (top horizontal axis) of the ^{41}K^{87}Rb TEDM relevant for the [B-c] STIRAP scheme through $\Omega = 1$ excited states. The pump transition starts from the $v_a = 29$ level of $a^3\Sigma^+$, towards vibrational levels v_1' of the $B^1\Pi$, $c^3\Sigma^+$, and $b^3\Pi$ coupled states located well below the K($4^2S_{1/2}$) + Rb($5^2P_{1/2}$) limit. The curves for $j_t = c$ (red solid circles) and $j_t = b$ (open black circles) are displayed. The dump transition (blue triangles) starts from those levels to end at the $v = 0$ level of the $X^1\Sigma^+$ ground state. (b) Magnification of the region of the most favorable intermediate coupled levels. The $v_1' = 101$ and $v_1' = 165$ are the optimal intermediate levels predicted by our calculations. The level $v_1' = 96$ (assigned to $v_1'^c = 23$) is analogous to the one used in the experiment of Ref. [61] with Feshbach ^{40}K^{87}Rb molecules. The $v_1' = 146$ and $v_1' = 152$ levels exhibit a strong mixture of $v_1'^B =\sim 7$–8 and $v_1'^c =\sim 48$–50 and could result in optimal STIRAP transfer in ^{39}K^{85}Rb [84].

in this range of distances [Fig. 1(f)]. The lowest $B^1\Pi$ levels $v_1'^{(B)}$ are reached when $E_{\rm dump} \sim 15\,000$ cm^{-1}, leading to a further increase of $|d_{BX}^{v_1' 0}|^2$ by two orders of magnitude for several coupled levels ($v_1' = 120, 124, 127, 132, 136$), assigned to $v_1'^{(B)} = 0,1,2,3,4$. The decrease for higher dump energies above $\sim$15 700 cm^{-1} is not significant because the avoided crossing between the $B^1\Pi$ PEC and the next $(2)^1\Pi$ PEC (not represented in Fig. 1) is not included in our model. Note that this avoided crossing results in a huge drop of the $d_{XB}(R)$ down to small magnitude beyond this distance.

The identification of an optimal intermediate level for the STIRAP scheme will then concern levels with mainly c and B character, chosen in the pump and dump energy range depicted in Fig. 3(b). In the following, we focus our study on three cases. We first look for the optimal intermediate levels starting with molecules initially in the $v_a = 29$ level. Then we analyze the experimental predictions for optimal STIRAP predicted in ^{39}K^{85}Rb for molecules produced through PA in the $v_a = 21$ level [84] and extend these "spectroscopic" predictions to other KRb molecules. Finally, we discuss the efficiency of a STIRAP process transferring $v_a = 29$ molecules into $v = 0$ through the optimal intermediate level of the second case above.

B. Identification of the optimal intermediate Ω = 1 levels for STIRAP

The characteristic of such levels are summarized in Table IV for the ^{39}K^{85}Rb and ^{39}K^{87}Rb isotopologues and in Table V for the ^{40}K^{87}Rb and ^{41}K^{87}Rb isotopologues. As previously stated, two initial $a^3\Sigma^+$ levels are considered, $v_a = 21,29$. In addition, we report in Table VI the levels which are involved in the available experimental results, which we tentatively characterize through our theoretical model.

Starting from $v_a = 29$, two sets of optimal levels are identified for the four molecules. First the levels $v_1' \sim 100$ are located in the $E_{\rm dump} \sim 14\,625$–$14\,675$ cm^{-1} range—below the minimum of the $B^1\Pi$ PEC—and are assigned to $v_1'^{(c)} = 25$ or 26 with a dominant $c^3\Sigma^+$ character. An equivalent efficiency of the STIRAP process is predicted if it relies on the intermediate levels $v_1' \sim 162$–165 around $E_{\rm dump} \sim 15\,670$ cm^{-1}, now above the $B^1\Pi$ minimum, presenting a strong mixture of c and B character, but for which a tentative assignment to $v_1'^{(c)}$ levels is proposed.

It is worthwhile to note that our predicted level $v_1' = 99$ in ^{40}K^{87}Rb results in a STIRAP scheme very similar to the one used in Ref. [61]. In this experiment, the intermediate level $v_1'^{(c)} = 23$ has been used to transform Feshbach molecules from $v_a = 30$ (or $\overline{v}_a = -2$) into $v = 0$ ground-state molecules. This assignment is provided by the theoretical analysis of Ref. [77] based on another set of *ab initio* potentials from Ref. [81], which also calculated a squared TME for the dump transition in very good agreement with the measured value. In our model this level is assigned to $v_1' = 95$ and presents a balanced mixture of b and c states (see Table VI). Clearly, the description of the strongly mixed $v' = 95$ level is very sensitive to the details in the PECs, preventing a more detailed interpretation of the observations. We ensured, however, that using our v_1' intermediate level to transfer ^{40}K^{87}Rb molecules from the $v_a = 30$ (or $\overline{v}_a = -2$) level leads to well-balanced TMEs of $|d_{ca}^{v_1' v_a}|^2 = 0.002$ a.u. and $|d_{BX}^{v_1' 0}|^2 = 0.0048$ a.u. (and a negligible $|d_{ba}^{v_1' v_a}|^2 = 5 \times 10^{-7}$ a.u.)

As a test of our model, we report in Table VI the characteristics of the intermediate levels predicted by our calculations for the STIRAP scheme determined from the spectroscopic analysis of Refs. [84,85]. Starting from $v_a = 21$, the intermediate levels are assigned to $v_1'^{(B)} = 7,8$, strongly mixed to neighboring $v'^{(c)}$ and $v'^{(b)}$ levels, resulting in a set of four levels $v' = 145,146,149$, and 150 (indexed by α, β, γ, and δ) in the table. We see that our calculated weights justify such an assignment. Their calculated energies are in

TABLE IV. Summary of the characteristics of the optimal transitions for the [B-c] STIRAP scheme through $\Omega = 1$ intermediate levels v_1' in ^{39}K^{85}Rb and ^{39}K^{87}Rb. Pump transition from $a^3\Sigma^+$ levels $v_a = 29$ (simulating a Feshbach molecule) and $v_a = 21$ (populated by PA in Ref. [84]) are considered. The dump transition ends at $v = 0$ of the $X^1\Sigma^+$state. Both binding energy $E_{\rm bind}$ [relative to the K($4s$) + Rb($5p$) dissociation limit] and excitation energy $E_{\rm exc}$ (relative to the minimum of the $X^1\Sigma^+$ potential well) of the v_1' levels are given, with the weight of the B, c, and b components [Eq. (3)]. The energies $E_{\rm pump}$ and $E_{\rm dump}$ and the related squared transition dipole moments of the pump and dump transitions are also reported. The intermediate levels $v_1'^{(c)} = 48$ and $v_1'^{(B)} = 8$ correspond the pump transition proposed in Ref. [84] for ^{39}K^{85}Rb, starting from $v_a = 21$. The same scheme also holds for ^{39}K^{87}Rb with $v_1'^{(c)} = 44$ and $v_1'^{(B)} = 8$. These levels are found to be suitable for a STIRAP transfer when starting from $v_a = 29$. Numbers in parentheses hold for powers of 10.

Initial level	^{39}K^{85}Rb						^{39}K^{87}Rb					
v_a	2 9				2 1		2 9				2 1	
Intermediate level												
v_1'	100	162	145	149	145	149	98	162	145	149	145	149
$v_1'^{(c)}$	26	55	48		48		26	59	44		44	
$v_1'^{(B)}$				8		8				8		8
$E_{\rm bind}$ (cm^{-1})	2280.6	1272.8	1501.1	1441.6	1501.1	1441.6	2329.7	1278.0	1505.7	1446.5	1505.7	1446.5
$E_{\rm exc}$ (cm^{-1})	14 674.6	15 682.4	15 454.1	15 513.6	15 454.1	15 513.6	14 625.5	15 677.2	15 449.4	15 508.6	15 449.4	15 508.6
$\varpi_b^{1v_1'}$	0.271	0.071	0.040	0.042	0.040	0.042	0.314	0.170	0.061	0.161	0.061	0.161
$\varpi_c^{1v_1'}$	0.726	0.566	0.584	0.463	0.584	0.463	0.683	0.416	0.651	0.532	0.651	0.532
$\varpi_B^{1v_1'}$	0.003	0.363	0.376	0.495	0.376	0.495	0.003	0.413	0.288	0.307	0.288	0.307
Pump transition												
$E_{\rm pump}$ (cm^{-1})	10 457.0	11 464.8	11 236.5	11 296.0	11 251.1	11 310.6	10 407.9	11 459.6	11 231.9	11 291.1	11 246.8	11 306.0
$\lvert d_{ca}^{v_1'v_a}\rvert^2$ (a.u.)	6.29(−3)	6.19(−3)	1.73(−3)	2.64(−3)	4.17(−2)	6.37(−2)	5.62(−3)	4.73(−3)	1.44(−3)	3.57(−3)	4.66(−2)	8.36(−2)
$\lvert d_{ba}^{v_1'v_a}\rvert^2$ (a.u.)	5.23(−7)	6.31(−8)	5.46(−7)	1.43(−9)	3.01(−7)	4.74(−6)	5.78(−7)	1.99(−6)	1.40(−6)	2.75(−6)	6.11(−6)	9.18(−6)
Dump transition												
$E_{\rm dump}$ (cm^{-1})	14 636.7	15 644.5	15 416.2	15 475.8	15 416.2	15 475.8	14 587.8	15 639.5	15 411.7	15 470.9	15 411.7	15 470.9
$\lvert d_{BX}^{v_1'v}\rvert^2$ (a.u.)	7.93(−3)	6.58(−3)	1.08(−1)	6.80(−2)	1.08(−1)	6.80(−2)	7.30(−3)	6.10(−3)	7.39(−2)	3.64(−2)	7.39(−2)	3.64(−2)

good agreement with the experimental ones, especially for the levels α ($v'^{(c)} = 44$) and γ ($v'^{(B)} = 8$) with theoretical energy higher then the experimental ones by only 1.07 and 1.70 cm^{-1}, respectively. The calculated TMEs confirm that these four levels are suitable for implementing an efficient STIRAP, while it is hard to reproduce the experimentally determined TMEs. These levels lie in an energy domain only 220 to 250 cm^{-1} below the upper optimal energy domain identified with our model. In Tables IV and V we extended the modeling of this scheme for the four isotopologues, starting

TABLE V. Same as Table IV for the ^{40}K^{87}Rb and ^{41}K^{87}Rb isotopologues.

Initial level	^{40}K^{87}Rb						^{41}K^{87}Rb					
a v_a	2 9				2 1		2 9				2 1	
Intermediate level												
v_1'	99	164	146	151	146	151	101	165	146	152	146	152
$v_1'^{(c)}$	25	55	47		47		26	56	48		48	
$v_1'^{(B)}$				8		8				8		8
$E_{\rm bind}$ (cm^{-1})	2327.9	1269.0	1513.6	1440.9	1513.6	1440.9	2303.5	1279.5	1529.2	1447.2	1529.2	1447.2
$E_{\rm exc}$ (cm^{-1})	14 627.3	15 686.2	15 441.5	15 514.3	15 441.5	15 514.3	14 651.7	15 675.7	15 426.0	15 508.0	15 426.0	15 508.0
$\varpi_b^{1v_1'}$	0.413	0.212	0.421	0.099	0.421	0.099	0.262	0.051	0.088	0.057	0.088	0.057
$\varpi_c^{1v_1'}$	0.586	0.558	0.509	0.431	0.509	0.431	0.735	0.669	0.810	0.378	0.810	0.378
$\varpi_B^{1v_1'}$	0.002	0.230	0.070	0.470	0.070	0.470	0.003	0.279	0.102	0.565	0.102	0.565
Pump transition												
$E_{\rm pump}$ (cm^{-1})	10 409.8	11 468.7	11 224.1	11 296.8	11 239.6	11 312.4	10 434.3	11 458.3	11 208.6	11 290.6	11 224.8	11 306.8
$\lvert d_{ca}^{v_1'v_a}\rvert^2$ (a.u.)	4.32(−3)	5.46(−3)	9.76(−4)	5.26(−3)	5.30(−2)	4.41(−2)	8.26(−3)	6.84(−3)	6.02(−4)	5.51(−3)	6.79(−2)	2.43(−2)
$\lvert d_{ba}^{v_1'v_a}\rvert^2$ (a.u.)	1.3(−6)	7.94(−6)	2.6(−6)	2.46(−6)	6.55(−5)	1.15(−6)	8.65(−7)	2.76(−7)	2.1(−6)	1.7(−7)	1.8(−6)	9.0(−6)
Dump transition												
$E_{\rm dump}$ (cm^{-1})	14 589.9	15 648.8	15 404.1	15 476.9	15 404.1	15 476.9	14 614.6	15 638.6	15 388.9	15 470.9	15 388.9	15 470.9
$\lvert d_{BX}^{v_1'v}\rvert^2$ (a.u.)	4.84(−3)	5.1(−3)	1.4(−2)	7.7(−2)	1.4(−2)	7.7(−2)	7.64(−3)	6.54(−3)	3.2(−3)	9.4(−2)	3.2(−3)	9.4(−2)

TABLE VI. Energies of the coupled $\Omega = 1$ levels v_1' assigned from the present model and involved in the experimentally investigated STIRAP processes. The experimental assignment in terms of levels of the c or B state is given, together the calculated weights $\varpi_b^{1v_1'}$, $\varpi_B^{1v_1'}$, and $\varpi_c^{1v_1'}$. The calculated squared TMEs for the pump and dump transitions are reported and compared to the experimental data. Two isotopologues are addressed: the $^{40}K^{87}Rb$ one for which an optimal STIRAP process has been successfully achieved [61] (the estimate provided by Ref. [77] for the dump transition in $^{40}K^{87}Rb$ is also reported); the $^{39}K^{85}Rb$ one for which optimal STIRAP processes have been predicted in [84] relying on the intermediate level α, β, γ, or δ (see text). For these levels the product of the intensities of the pump and dump transitions is the largest. Numbers in parentheses hold for powers of 10.

Initial level	Ref.	Exp. assigned level	Calc.v_1'	Energy (cm^{-1})	$\varpi_b^{1v_1'}$	$\varpi_B^{1v_1'}$	$\varpi_c^{1v_1'}$	$\lvert d_{ca}^{v_1'v_a}\rvert^2$ (a.u.)	$\lvert d_{BX}^{v_1'v}\rvert^2$ (a.u.)
$^{40}K^{87}Rb$	This work		95	14 540.21	0.478	0.002	0.520	6.0(−4)	3.1(−3)
	Exp. [61]	$v_1'^{(c)} = 23$		14 545.01				2.5(−5)	1.44(−4)
$v_a = 30$	Theor. [77]				0.210	0.002	0.788		3.24 (−4)
	This work		145	15 454.07	0.040	0.376	0.584	0.0417	0.1078
$^{39}K^{85}Rb$	Exp. [84,97]	$\alpha : v_1'^{(c)} = 44$		15 452.99				1.1	0.6
	This work		146	15 466.78	0.038	0.521	0.441	0.0347	0.1510
	Exp. [84,97]	$\beta : v_1'^{(B)} = 7$		15 459.55				1.9	0.5
$v_a = 21$									
	This work		149	15 513.61	0.042	0.495	0.463	0.0637	0.0680
	Exp. [84,97]	$\gamma : v_1'^{(B)} = 8$		15 511.90				1.4	0.8
	This work		150	15 524.84	0.354	0.244	0.402	0.0520	0.0367
	Exp. [84,97]	$\delta : v_1'^{(c)} = 46$		15 520.21				0.7	0.9

from $v_a = 21$ and involving the analogous α and γ levels with calculated energies close to the experimental ones. Results for levels lying in this favorable energy domain, for example, for the β and δ levels, are available in the Supplemental Material attached to the present paper [91]. This demonstrates that this favorable STIRAP scheme is general and can be applied to all KRb isotopologues.

Finally, we predict that the above intermediate levels α and γ are also suitable for transferring $v_a = 29$ molecules into $v = 0$ ground-state molecules for all isotopologues. Their characteristics are reported in Table IV for $^{39}K^{85}Rb$ and $^{39}K^{87}Rb$ ($v_1' = 145, 149$) and in Table V for $^{40}K^{87}Rb$ and $^{41}K^{87}Rb$ ($v_1' = 146, 151$ and $v_1' = 146, 152$, respectively).

VI. CONCLUDING REMARKS

Experimental results are often obtained before a complete theoretical modeling of the physical system under study is available. This is undoubtedly the case for the demonstration of the first STIRAP transfer scheme achieved on ultracold KRb Feshbach molecules by Ni *et al.* [61], relying on a partial knowledge of the KRb molecular structure. By collecting all the available spectroscopic and theoretical data on this molecule, the present paper delivers a complete view of the current knowledge of the KRb spectroscopy. This study confirms the results of Ref. [61], that is the efficiency of the [B-c] scheme used by the authors to set up their STIRAP transfer. The additional knowledge brought by Kim *et al.* [84] allowed us to predict a STIRAP scheme relying on molecular transitions which is expected to be 100 times more intense than the one used in Ref. [61].

Moreover, our results confirm the superiority of the [B-c] STIRAP scheme compared to the [b-A] STIRAP scheme which was previously used in Cs_2 [66] and explored later on RbCs by the same group [69,105]. Despite favorable FC factors for the pump step of the [b-A] scheme, the TEDM for the upward $a^3\Sigma^+ \rightarrow b^3\Pi$ transition around the inner turning point of the $a^3\Sigma^+$ potential (located at $R_a \sim 9$ a.u.) is surprisingly small, i.e., 0.028 a.u. [83]. This induces a very weak pump transition most often strongly imbalanced with the downward $X^1\Sigma^+ \rightarrow A^1\Sigma^+$ transition of the [b-A] scheme. However, such a situation is probably not applicable to the entire series of heteronuclear alkali-metal diatomics. Indeed, as reported in Ref. [107], the electronic transition dipole moment for the same transition in NaK, NaRb, and NaCs amounts to about 0.85 a.u. at the same internuclear distance of 9 a.u., which still corresponds to the inner turning point of the $a^3\Sigma^+$ potential curve. Therefore, for these molecules, the [b-A] STIRAP scheme is expected to rely on upward vibrational transitions which are about 1000 times stronger than for KRb. Such a result should be of interest for the ongoing experiments with these molecules [57,58].

ACKNOWLEDGMENTS

We are indebted to Professor G. Modugno and Dr. S. Chauduri from the LENS, Università di Firenze, for sharing with us their interest in producing and manipulating bosonic $^{39}K^{87}Rb$ molecules in 3D optical lattices, which is at the origin of the present study. We thank M. Aymar for fruitful discussions about potential curves and electronic dipole transition moments. Laboratoire Aimé Cotton is "unité propre UPR 3321 du CNRS associé à l'Université Paris-Sud," member of "Fédération Lumière Matière" (LUMAT, FR2764) and the "Institut Francilien de Recherche sur les Atomes Froids" (IFRAF).

[1] M. Anderson, J. Ensher, M. Matthews, C. Wieman, and E. Cornell, Science **269**, 198 (1995).

[2] K. B. Davis, M. O. Mewes, M. R. Andrews, N. J. van Druten, D. S. Durfee, D. M. Kurn, and W. Ketterle, Phys. Rev. Lett. **75**, 3969 (1995).

[3] C. C. Bradley, C. A. Sackett, J. J. Tollett, and R. G. Hulet, Phys. Rev. Lett. **75**, 1687 (1995).

[4] B. DeMarco and D. S. Jin, Science **285**, 1703 (1999).

[5] M. A. Baranov, Phys. Rep. **464**, 71 (2008).

[6] T. Lahaye, C. Menotti, L. Santos, M. Lewenstein, and T. Pfau, Rep. Prog. Phys. **72**, 126401 (2009).

[7] J. Stuhler, A. Griesmaier, T. Koch, M. Fattori, T. Pfau, S. Giovanazzi, P. Pedri, and L. Santos, Phys. Rev. Lett. **95**, 150406 (2005).

[8] G. Bismut, B. Laburthe-Tolra, E. Maréchal, P. Pedri, O. Gorceix, and L. Vernac, Phys. Rev. Lett. **109**, 155302 (2012).

[9] K. Aikawa, A. Frisch, M. Mark, S. Baier, A. Rietzler, R. Grimm, and F. Ferlaino, Phys. Rev. Lett. **108**, 210401 (2012).

[10] M. Lu, N. Q. Burdick, S. H. Youn, and B. L. Lev, Phys. Rev. Lett. **107**, 190401 (2011).

[11] L. D. Carr and J. Ye, New J. Phys. **11**, 055009 (2009).

[12] O. Dulieu and C. Gabbanini, Rep. Prog. Phys. **72**, 086401 (2009).

[13] D. Jin and J. Ye, Chem. Rev. **112**, 4801 (2012).

[14] M. Aymar and O. Dulieu, J. Chem. Phys. **122**, 204302 (2005).

[15] D. DeMille, F. Bay, S. Bickman, D. Kawall, D. Krause, Jr., S. E. Maxwell, and L. R. Hunter, Phys. Rev. A **61**, 052507 (2000).

[16] J. J. Hudson, B. E. Sauer, M. R. Tarbutt, and E. A. Hinds, Phys. Rev. Lett. **89**, 023003 (2002).

[17] D. M. Kara, I. J. Smallman, J. J. Hudson, B. E. Sauer, M. R. Tarbutt, and E. A. Hinds, New J. Phys. **14**, 103051 (2012).

[18] S. Eckel, P. Hamilton, E. Kirilov, H. W. Smith, and D. DeMille, Phys. Rev. A **87**, 052130 (2013).

[19] The ACME Collaboration, J. Baron, W. C. Campbell, D. DeMille, J. M. Doyle, G. Gabrielse, Y. V. Gurevich, P. W. Hess, N. R. Hutzler, E. Kirilov, I. Kozyryev *et al.*, Science **343**, 269 (2014).

[20] E. A. Hinds and P. G. H. Sandars, Phys. Rev. A **21**, 480 (1980).

[21] S. Schiller and V. Korobov, Phys. Rev. A **71**, 032505 (2005).

[22] V. I. Korobov, L. Hilico, and J.-P. Karr, Phys. Rev. Lett. **112**, 103003 (2014).

[23] C. Chin, V. V. Flambaum, and M. G. Kozlov, New J. Phys. **11**, 055048 (2009).

[24] D. DeMille, Phys. Rev. Lett. **88**, 067901 (2002).

[25] S. Yelin, R. Côté, and D. DeMille, *Quantum Information Processing with Ultracold Polar Molecules* (CRC Press, Boca Raton, FL, 2009), p. 629.

[26] R. V. Krems, Phys. Chem. Chem. Phys. **10**, 4079 (2008).

[27] A. Fioretti, D. Comparat, A. Crubellier, O. Dulieu, F. Masnou-Seeuws, and P. Pillet, Phys. Rev. Lett. **80**, 4402 (1998).

[28] E. S. Shuman, J. F. Barry, and D. DeMille, Nature (London) **467**, 820 (2010).

[29] J. F. Barry, E. S. Shuman, E. B. Norrgard, and D. DeMille, Phys. Rev. Lett. **108**, 103002 (2012).

[30] M. T. Hummon, M. Yeo, B. K. Stuhl, A. L. Collopy, Y. Xia, and J. Ye, Phys. Rev. Lett. **110**, 143001 (2013).

[31] J. Kobayashi, K. Aikawa, K. Oasa, and S. Inouye, Phys. Rev. A **89**, 021401 (2014).

[32] H. R. Thorsheim, J. Weiner, and P. S. Julienne, Phys. Rev. Lett. **58**, 2420 (1987).

[33] W. Stwalley and H. Wang, J. Mol. Spectrosc. **195**, 194 (1999).

[34] K. M. Jones, E. Tiesinga, P. D. Lett, and P. S. Julienne, Rev. Mod. Phys. **78**, 483 (2006).

[35] D. Wang, J. Qi, M. F. Stone, O. Nikolayeva, B. Hattaway, S. D. Gensemer, H. Wang, W. T. Zemke, P. L. Gould, E. E. Eyler *et al.*, Eur. Phys. J. D **31**, 165 (2004).

[36] M. W. Mancini, G. D. Telles, A. R. L. Caires, V. S. Bagnato, and L. G. Marcassa, Phys. Rev. Lett. **92**, 133203 (2004).

[37] J. Banerjee, D. Rahmlow, R. Carollo, M. Bellos, E. E. Eyler, P. L. Gould, and W. C. Stwalley, Phys. Rev. A **86**, 053428 (2012).

[38] A. J. Kerman, J. M. Sage, S. Sainis, T. Bergeman, and D. DeMille, Phys. Rev. Lett. **92**, 153001 (2004).

[39] J. M. Sage, S. Sainis, T. Bergeman, and D. DeMille, Phys. Rev. Lett. **94**, 203001 (2005).

[40] C. Gabbanini and O. Dulieu, Phys. Chem. Chem. Phys. **13**, 18905 (2011).

[41] S. D. Kraft, P. Staanum, J. Lange, L. Vogel, R. Wester, and M. Weidemüller, J. Phys. B **39**, S993 (2006).

[42] J. Deiglmayr, M. Aymar, R. Wester, M. Weidemüller, and O. Dulieu, J. Chem. Phys. **129**, 064309 (2008).

[43] C. Haimberger, J. Kleinert, M. Bhattacharya, and N. F. Bigelow, Phys. Rev. A **70**, 021402(R) (2004).

[44] S. Dutta, D. S. Elliott, and Y. P. Chen, Europhys. Lett. **104**, 63001 (2013).

[45] K. Bergmann, H. Theuer, and B. W. Shore, Rev. Mod. Phys. **70**, 1003 (1998).

[46] N. V. Vitanov, M. Fleischhauer, B. W. Shore, and W. Bergemann, Adv. At. Mol. Opt. Phys. **46**, 55 (2001).

[47] K. Aikawa, D. Akamatsu, M. Hayashi, K. Oasa, J. Kobayashi, P. Naidon, T. Kishimoto, M. Ueda, and S. Inouye, Phys. Rev. Lett. **105**, 203001 (2010).

[48] E. Tiesinga, B. J. Verhaar, and H. T. C. Stoof, Phys. Rev. A **47**, 4114 (1993).

[49] T. Köhler, K. Góral, and P. S. Julienne, Rev. Mod. Phys. **78**, 1311 (2006).

[50] C. Chin, R. Grimm, P. Julienne, and E. Tiesinga, Rev. Mod. Phys. **82**, 1225 (2010).

[51] C. A. Stan, M. W. Zwierlein, C. H. Schunck, S. M. F. Raupach, and W. Ketterle, Phys. Rev. Lett. **93**, 143001 (2004).

[52] S. Inouye, J. Goldwin, M. L. Olsen, C. Ticknor, J. L. Bohn, and D. S. Jin, Phys. Rev. Lett. **93**, 183201 (2004).

[53] K. Pilch, A. D. Lange, A. Prantner, G. Kerner, F. Ferlaino, H.-C. Nägerl, and R. Grimm, Phys. Rev. A **79**, 042718 (2009).

[54] M. Repp, R. Pires, J. Ulmanis, R. Heck, E. D. Kuhnle, M. Weidemüller, and E. Tiemann, Phys. Rev. A **87**, 010701(R) (2013).

[55] H.-W. Cho, D. J. McCarron, M. P. Köppinger, D. L. Jenkin, K. L. Butler, P. S. Julienne, C. L. Blackley, C. R. Le Sueur, J. M. Hutson, and S. L. Cornish, Phys. Rev. A **87**, 010703 (2013).

[56] E. Wille, F. M. Spiegelhalder, G. Kerner, D. Naik, A. Trenkwalder, G. Hendl, F. Schreck, R. Grimm, T. G. Tiecke, J. T. M. Walraven *et al.*, Phys. Rev. Lett. **100**, 053201 (2008).

[57] C.-H. Wu, J. W. Park, P. Ahmadi, S. Will, and M. W. Zwierlein, Phys. Rev. Lett. **109**, 085301 (2012).

[58] F. Wang, D. Xiong, X. Li, D. Wang, and E. Tiemann, Phys. Rev. A **87**, 050702 (2013).

[59] B. Deh, C. Marzok, C. Zimmermann, and P. W. Courteille, Phys. Rev. A **77**, 010701 (2008).

[60] C. Marzok, B. Deh, C. Zimmermann, P. W. Courteille, E. Tiemann, Y. V. Vanne, and A. Saenz, Phys. Rev. A **79**, 012717 (2009).

[61] K.-K. Ni, S. Ospelkaus, M. H. G. de Miranda, A. Peer, B. Neyenhuis, J. J. Zirbel, S. Kotochigova, P. S. Julienne, D. S. Jin, and J. Ye, Science **322**, 231 (2008).

[62] A.-C. Voigt, M. Taglieber, L. Costa, T. Aoki, W. Wieser, T. W. Hänsch, and K. Dieckmann, Phys. Rev. Lett. **102**, 020405 (2009).

[63] T. Takekoshi, M. Debatin, R. Rameshan, F. Ferlaino, R. Grimm, H.-C. Naegerl, C. Le Sueur, J. Hutson, P. Julienne, S. Kotochigova, and E. Tiemann, Phys. Rev. A **85**, 032506 (2012).

[64] M. P. Köppinger, D. J. McCarron, D. L. Jenkin, P. K. Molony, H.-W. Cho, S. L. Cornish, C. R. Le Sueur, C. L. Blackley, and J. M. Hutson, Phys. Rev. A **89**, 033604 (2014).

[65] M.-S. Heo, T. T. Wang, C. A. Christensen, T. M. Rvachov, D. A. Cotta, J.-H. Choi, Y.-R. Lee, and W. Ketterle, Phys. Rev. A **86**, 021602 (2012).

[66] J. G. Danzl, E. Haller, M. Gustavsson, M. J. Mark, R. Hart, N. Bouloufa, O. Dulieu, H. Ritsch, and H.-C. Nägerl, Science **321**, 1062 (2008).

[67] F. Lang, K. Winkler, C. Strauss, R. Grimm, and J. Hecker Denschlag, Phys. Rev. Lett. **101**, 133005 (2008).

[68] J. J. Zirbel, K.-K. Ni, S. Ospelkaus, T. L. Nicholson, M. L. Olsen, P. S. Julienne, C. E. Wieman, J. Ye, and D. S. Jin, Phys. Rev. A **78**, 013416 (2008).

[69] T. Takekoshi, L. Reichsöllner, A. Schindewolf, J. M. Hutson, C. R. L. Sueur, O. Dulieu, F. Ferlaino, R. Grimm, and H.-C. Nägerl, arXiv:1405.6037.

[70] V. Kokoouline, O. Dulieu, R. Kosloff, and F. Masnou-Seeuws, J. Chem. Phys. **110**, 9865 (1999).

[71] A. J. Ross, C. Effantin, P. Crozet, and E. Boursey, J. Phys. B **23**, L247 (1990).

[72] N. Okada, S. Kasahara, T. Ebi, M. Baba, and H. Katô, J. Chem. Phys. **105**, 3458 (1996).

[73] S. Kasahara, C. Fujiwara, N. Okada, H. Katô, and M. Baba, J. Chem. Phys. **111**, 8857 (1999).

[74] C. Amiot and J. Vergès, J. Chem. Phys. **112**, 7068 (2000).

[75] C. Amiot and J. Vergès, J. Mol. Spectrosc. **203**, 126 (2000).

[76] A. Pashov, O. Docenko, M. Tamanis, R. Ferber, H. Knöckel, and E. Tiemann, Phys. Rev. A **76**, 022511 (2007).

[77] S. Kotochigova, E. Tiesinga, and P. S. Julienne, New J. Phys. **11**, 055043 (2009).

[78] A. Yiannopoulou, T. Leininger, A. M. Lyyra, and G.-H. Jeung, Int. J. Quant. Chem. **57**, 575 (1996).

[79] T. Leininger, H. Stoll, and G.-H. Jeung, J. Chem. Phys. **106**, 2541 (1997).

[80] S. Park, Y. J. Choi, Y. S. Lee, and G.-H. Jeung, Chem. Phys. **257**, 135 (2000).

[81] S. Rousseau, A. R. Allouche, and M. Aubert-Frécon, J. Mol. Spectrosc. **203**, 235 (2000).

[82] S. Kotochigova, P. S. Julienne, and E. Tiesinga, Phys. Rev. A **68**, 022501 (2003).

[83] R. Beuc, M. Movre, T. Ban, G. Pichler, M. Aymar, O. Dulieu, and W. E. Ernst, J. Phys. B **39**, S1191 (2006).

[84] J.-T. Kim, Y. Lee, B. Kim, D. Wang, W. C. Stwalley, P. L. Gould, and E. E. Eyler, Phys. Rev. A **84**, 062511 (2011).

[85] W. C. Stwalley, M. Bellos, J. Banerjee, and M. Bermudez, Mol. Phys. **110**, 1739 (2012).

[86] J. T. Kim, Y. Lee, B. Kim, D. Wang, P. L. Gould, E. E. Eyler, and W. C. Stwalley, J. Chem. Phys. **137**, 024301 (2012).

[87] K.-K. Ni, Ph.D. thesis, University of Colorado, 2009, available at http://jila.colorado.edu/~jin/publications/pdf/KangKuenThesis.pdf

[88] K. Aikawa, Ph.D. thesis, The University of Tokyo, Japan, 2011, available at http://ultracold.t.u-tokyo.ac.jp/inouyeLAB/publications/2011_Aikawa_PhD.pdf

[89] P. S. Julienne, Faraday Discuss. **142**, 361 (2009).

[90] S. Ospelkaus, A. Peer, K.-K. Ni, J. J. Zirbel, B. Neyenhuis, S. Kotochigova, P. S. Julienne, J. Ye, and D. S. Jin, Nat. Phys. **4**, 622 (2008).

[91] See Supplemental Material at http://link.aps.org/supplemental/10.1103/PhysRevA.90.033413 for the energy levels and squared transition matrix elements for the STIRAP schemes with $|i\rangle = |a, v_a = 20\text{–}31\rangle$ for the most commonly studied isotopologues $^{39}K^{85}Rb$, $^{39}K^{87}Rb$, $^{40}K^{87}Rb$, and $^{41}K^{87}Rb$.

[92] M. Tscherneck and N. P. Bigelow, Phys. Rev. A **75**, 055401 (2007).

[93] W. C. Stwalley, Eur. Phys. J. D **31**, 221 (2004).

[94] R. Beuc, M. Movre, V. Horvatic, C. Vadla, O. Dulieu, and M. Aymar, Phys. Rev. A **75**, 032512 (2007).

[95] K. Willner, O. Dulieu, and F. Masnou-Seeuws, J. Chem. Phys. **120**, 548 (2004).

[96] B. Gao, E. Tiesinga, C. J. Williams, and P. S. Julienne, J. Phys. B **37**, 4273 (2004).

[97] J. T. Kim, Y. Lee, B. Kim, D. Wang, W. C. Stwalley, P. L. Gould, and E. Eyler, Phys. Chem. Chem. Phys. **13**, 18755 (2011).

[98] M. Marinescu and H. R. Sadeghpour, Phys. Rev. A **59**, 390 (1999).

[99] F. Ferlaino, C. D'Errico, G. Roati, M. Zaccanti, M. Inguscio, G. Modugno, and A. Simoni, Phys. Rev. A **74**, 039903 (2006).

[100] D. Wang, J. T. Kim, C. Ashbaugh, E. E. Eyler, P. L. Gould, and W. C. Stwalley, Phys. Rev. A **75**, 032511 (2007).

[101] M. Aymar and O. Dulieu, J. Chem. Phys. **125**, 047101 (2006).

[102] G.-H. Jeung, J. Mol. Spectrosc. **182**, 113 (1997).

[103] S. Azizi, Ph.D. thesis, Université Paris-Sud (France), 2006.

[104] O. Docenko, M. Tamanis, R. Ferber, E. A. Pazyuk, A. Zaitsevskii, A. V. Stolyarov, A. Pashov, H. Knöckel, and E. Tiemann, Phys. Rev. A **75**, 042503 (2007).

[105] M. Debatin, T. Takekoshi, R. Rameshan, L. Reichsoellner, F. Ferlaino, R. Grimm, R. Vexiau, N. Bouloufa, O. Dulieu, and H.-C. Naegerl, Phys. Chem. Chem. Phys. **13**, 18926 (2011).

[106] S. Ospelkaus, K.-K. Ni, G. Quéméner, B. Neyenhuis, D. Wang, M. H. G. deMiranda, J. L. Bohn, J. Ye, and D. S. Jin, Phys. Rev. Lett. **104**, 030402 (2010).

[107] M. Aymar and O. Dulieu, Mol. Phys. **105**, 1733 (2007).